INSIGHTS ON PIXEL AND SUB PIXEL SCALE ROCK ABUNDANCE ON THE MOON WITH LROC/NAC. R. Marshal[1], K. Wohlfarth[2], O. Ruesch[1], [1]Institut für Planetologie, Westfälische Wilhelms Universität Münster, Münster, Germany (rachael.marshal@uni-muenster.de). [2]Image Analysis Group, Technische Universität Dortmund, Dortmund, Germany.

Introduction: Surfaces of planetary bodies are abundant with rock fragments associated with impact crater ejecta [e.g., 1]. Under exposure to the space environment, rocks are shattered and comminuted [2]. Understanding rock fragmentation processes with time can be key to gain insight on the evolution of the regolith on the planetary body [2,3]. Studies of the size frequency distribution (SFD) [e.g., 1,3,4,5] as well as the morphology and abundance [6] of rock fragment families have been key in making inferences regarding the surface exposure age.

When employing an SFD for lunar rock fragments utilizing data from the Lunar Reconnaissance Orbiter Narrow Angle Camera (LROC/NAC) [7], a key limitation is the mapping of pixel and sub-pixel scale rock fragments. Most studies employ a cut off threshold at ~2 m, below which the detection and mapping of rock fragments become ambiguous due to spatial resolution (i.e., ground sampling dimension) constraints: at a minimum, three pixels are needed to identify a feature (3x0.5 m). The study of the meter and sub-meter scale lunar geology and topography can be particularly important in bringing forward a better link between returned lunar samples and remote sensing observations. Analysis of the local scale geology could be helpful in understanding how thermal fatigue as well as small impacts influence the lunar regolith [2] and how regolith can develop centimeter-scale cold traps [8]. In this study we aim at extracting information at the smallest possible spatial scale from LROC/NAC, i.e., at the sub-pixel scale.

Method: Variations of reflectance across an image can be considered to result from topographic variation within an area of constant albedo. With photoclinometry, such consideration can be applied even on pixel-to-pixel reflectance variations [9]. Here, instead, we consider cases where the pixel-to-pixel reflectance variations can result from differences in sub-pixel rock abundance. This approximation is likely to be sufficient for topographically flat surfaces that are known to host rocks and have very few small impact craters (e.g., very young surfaces). Spatially inhomogeneous albedo can be present in young surfaces that tend to be less affected by space weathering than the older parts of the surface. Albedo inhomogeneity, however, is unlikely to cause pixel-to-pixel variation. We first explore the image texture and pixel-to-pixel reflectance variability by calculating pixel scale roughness values [e.g., 10] around lunar landing sites with visually identifiable rocks. We implement this pixel scale roughness measurements by taking the reflectance differences between a pixel and its neighbors. In order to investigate the physical meaning of pixel scale roughness values, we generate a synthetic terrain to represent the topography due to rocks within each pixel. For our modelling process, we use a pre-derived cumulative areal fraction distribution [3] that defines the number of rocks of a given diameter. From these synthetic terrains we calculate mean reflectance values for a range of cumulative areal fraction of rocks (CAF). We model sub-pixel rocks as mounds [11] and use a Lunar Lambertian reflectance function [12]. The shadowed regions are calculated using the ray tracing technique.

Preliminary results: We calculated pixel-to-pixel roughness values for South Ray (~2 My), North Ray (~50 My) and Camelot (<140 My) craters. We find that roughness decreases with increasing surface exposure age. We find that the lowest modelled CAF of ~1 % causes an increase in reflectance of ~1 % compared to a topographically flat (CAF=0 %) pixel. A CAF of ~12 % causes an increase in reflectance of ~10 % compared to a flat pixel. At North Ray crater we find that CAF values greater than 12 % highlight multi pixel rocks. Single bright pixels, i.e., pixel with unresolved rocks, with a CAF values higher than 12 % are not found. Thus, at this site, there is a lack of rocks beyond the diameter of ~5 cm, the largest fragment for a CAF of 12 %. If the increase in reflectance (CAF of 12 %) is due to a single rock, instead of a family following the SFD of [3], the rock is on the order of ~18 cm wide. Therefore, the highest reflectance acquired by the camera and confined to a single pixel (~50x50 cm) is due to a single rock of diameter ~18 cm, or to several rocks of smaller diameters. Larger rocks in the range ~18–50 cm are not present.

The automatic classification of pixels has been visually verified with a comparison to the original NAC image. False positive pixels with high CAF have been found as part of blocks >10 pixels in size, at transition zones between illuminated and shadowed regions, and as part of recognized topographic features, e.g., few pixels wide impact craters. Overall, false positive are a minor fraction of all detections, so that density maps can be produced. Pixels with CAF 1-2% are found

throughout the study area (Figure 1) without any association to larger geological features. Pixels of higher CAF (~10-12 %) are clustered, for example near block fields (Figure 2). The high-density regions on the right end of Figure 1 and Figure 2 must be carefully interpreted since this region has a topographic descent owing to the fact that it lies on the rim and outer walls of the North Ray crater.

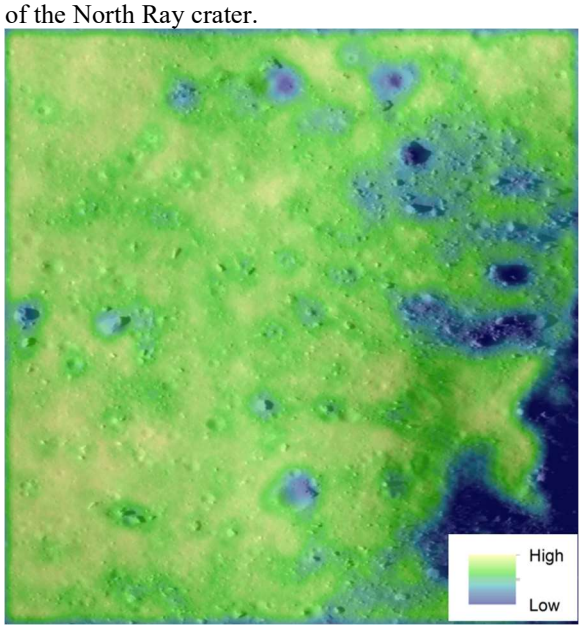

Figure 1: Density map of pixels with a cumulative areal fraction of sub-pixel rocks (CAF) of ~1 % on subset of image M129187331LC. The scene is 518 m wide.

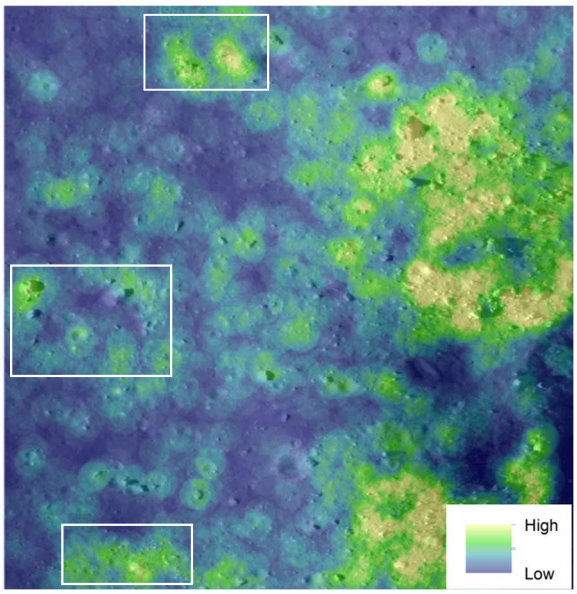

Figure 2: Density map of NAC pixels with a cumulative areal fraction of sub-pixel rocks (CAF) of ~10 % on subset of image M129187331LC. White boxes indicate CAF ~10 % pixels associated with spatially resolved block fields. The scene is 518 m wide.

Discussion and Conclusion: As expected, near lunar craters, the abundance of rocks of size below ~2 m decreases with increasing surface exposure age. Interestingly, the spatial distribution of these rocks depends on their size (Figure 1, Figure 2, and absence of rocks of ~18–50 cm), probably due to erosional and, possibly, formation processing that occurred after the emplacement of the first ejecta rocks population. At North Ray crater, the lack of rocks in the range ~18–50 cm confined to single pixels can be due to (i) the probability of a rock to contribute to multiple pixels increases as the size of the rock increases and (ii) the possible paucity of such large rocks in the study area due to erosional processes. The presence of sub-pixel rocks near blocks several meters wide (at block fields) could be explained by meteoroid impacts onto the large blocks with subsequent spalling and ejection of small fragments. Thus, these fragments might date well after the formation of North Ray crater. In general, few adjacent bright pixels in NAC images cannot always be interpreted as a block of ~1-2 m size (with 0.5 m/pixel): their reflectance can be explained by a much smaller rock that contributes to the brightness of multiple adjacent pixels. Thus, the measured size of blocks that extend only a few pixels in NAC images should be considered an upper estimate.

Future analysis will consider other CAF distributions [e.g., 3] and a representative camera system model, e.g., including a point spread function. Future comparisons can be performed with DIVINER (sub-meter) rock abundance along with comparison with the astronaut panoramas from the North Ray landing site. Improvements on density maps can be achieved using an integrated approach with high-resolution digital terrain models [e.g., 13]. A future application will be the estimation of sub pixel rock abundances at thermal anomaly cold spots [14] around very young craters.

Acknowledgments: R. M. and O. R. are supported by a Sofja Kovalevskaja Award of the Alexander von Humboldt Foundation.

References: [1] Basilevsky A.T. et al. (2013) *PSS, 89*, 118–126 [2] Hörz F. et al. (2020) *PSS, 194,*105105 [3] Watkins R.N. et al. (2019) *JGR-Planets, 124*, 2754–2771 [4] Bart G.D. and Melosh H.J. (2010) *Icarus, 209,* 337-357 [5] Di K. et al. (2016) *PSS 120*, 103–112 [6] Ruesch O. et al. (2020) *Icarus, 336,* 113431 [7] Robinson M.S. et al. (2010) *SSR, 150*, 81–124 [8] Hayne P.O. et al. (2020) *Nature Astronomy* [9] Kirk R.L. et al. (2003) *JGR-Planets, 108* [10] Tanabe N. et al. (2020) LPSC *LI, Abstract # 1800* [11] Gaskell R.W. (1993) *JGR, 98,* 11099-11103 [12] McEwen A.S. (1991) *Icarus, 92*, 298–311 [13] Grumpe A. et al., (2014), *Adv. Sp. Res. 53*, 1735-1767 [14] Hayne P.O. et al. (2017) *JGR-Planets 122*,2371–2400.